IOP Publishing | International Atomic Energy Agency Nuclear Fusion

Nucl. Fusion **57** (2017) 046013 (7pp) doi:10.1088/1741-4326/aa5cdf

The effect of inelastic collisions on the transport of alpha particles in ITER-like plasmas

C.F. Clauser[1,2] **and R. Farengo**[1]

[1] Centro Atómico Bariloche and Instituto Balseiro, Comisión Nacional de Energía Atómica and Universidad Nacional de Cuyo, Av. Bustillo 9500, 8400 Bariloche, Argentina
[2] Consejo Nacional de Investigaciones Científicas y Técnicas (CONICET), Argentina

E-mail: cesar.clauser@ib.edu.ar

Received 25 November 2016, revised 15 December 2016
Accepted for publication 25 January 2017
Published 24 February 2017

Abstract

The effect of charge changes on the transport of alpha particles in ITER-like plasmas is studied with a numerical code that follows the exact particle trajectories and includes the effect of elastic and inelastic collisions. It is shown that charge changing processes can produce significant changes in the transport of alpha particles in the edge-SOL region. The addition of inelastic collisions actually reduces the alpha particle loss rate below the level obtained when only elastic (Coulomb) collisions are included. This is due to the inward flux produced by the neutral density gradient. Power losses, on the other hand, remain at approximately the same level because the average energy of the lost particles is higher when inelastic collisions are included. Finally, the spatial distribution of the lost particles changes significantly when inelastic collisions are added, with a larger fraction of the lost particles reaching the wall.

Keywords: alpha particles, transport, inelastic collisions, particle simulation, ITER

(Some figures may appear in colour only in the online journal)

1. Introduction

The power deposited by the alpha particles produced in D-T reactions will be the main heating source available to compensate the losses and keep the plasma temperature constant. All the processes that affect the confinement of high energy alpha particles can therefore modify the performance of the reactor. On the other hand, low energy alpha particles (helium ash) must be removed to avoid the dilution of the fuel and the reduction of the fusion power. Coulomb collisions produce an unavoidable particle transport but other (‘anomalous’) processes can result in significantly higher transport rates. These include large scale MHD fluctuations, Alfvèn eigenmodes, microturbulence, toroidal ripple, and perturbations produced by ELM control coils.

Inelastic collisions, in particular collisions that change the charge state of the alpha particles, can also produce significant transport. This process, which we call ‘inelastic transport’, was first studied by Fussmann [1] who derived analytic expressions for the diffusion coefficient resulting from charge changes. When these equations were applied to alpha particles confined in the core of the reactor and subjected only to radiative recombination (RR) processes the diffusion coefficient resulted negligible.

We have recently presented analytical calculations and particle simulations that show that charge changing processes can significantly increase the diffusion of alpha particles in the pedestal-edge-SOL regions [2]. A simple 1D model was employed in [2], and only the interaction of the alpha particles with the plasma species, He^+ and neutral deuterium (both atomic and molecular) and helium were included. The cross sections of these processes were obtained from the existing databases [3] but it is clear that more, and more accurate, atomic data are needed.

The main conclusion of [2] is that once the alpha particles reach the pedestal region, charge changing processes become important and therefore calculations of the alpha particle flux to the wall and divertor should include them. Another important finding is the existence of an inward flux of alpha particles that further reduces their density near the separatrix, which is the region where the confinement can be significantly affected by the toroidal field ripple and the perturbations produced by ELM control coils.

Here we present new results, obtained with the same numerical code but a more realistic (2D) equilibrium and improved initial conditions. Classical (elastic) Coulomb collisions have been added, and this allows us to compare the results obtained when only elastic collisions are included with those obtained when both elastic and inelastic collisions are considered. We find that the addition of inelastic collisions actually reduces the alpha particle loss rate below the level obtained when only elastic (Coulomb) collisions are included. This is due to the inward flux produced by the neutral density gradient. Power losses, on the other hand, remain at approximately the same level because the average energy of the lost particles is higher when inelastic collisions are included. Finally, the spatial distribution of the lost particles changes significantly when inelastic collisions are added, with a larger fraction of the lost particles reaching the wall.

The structure of this paper is the following. In section 2 we introduce the numerical code employed. In section 3, we use the results obtained in a simple, 1D, case to discuss the basic physics of the transport produced by charge changes. In section 4, we introduce the 2D equilibrium employed (ITER inductive scenario) and the assumptions regarding the distribution of the alpha particles in velocity and configuration space. Section 5 contains the results of the simulations and section 6, the summary and conclusions.

2. Numerical code

The numerical code employed and the atomic processes included are the same as in [2]. The code calculates the exact alpha particle trajectories by solving Newton's equation with the Lorentz force and an additional term to account for the effect of elastic collisions,

$$\frac{\mathrm{d}\mathbf{v}}{\mathrm{d}t} = \frac{q(t)}{m}\mathbf{v}\times\mathbf{B} + \dot{\mathbf{v}}_{ec}, \tag{1}$$

where $\dot{\mathbf{v}}_{ec}$ is the elastic collision term [4] and $q(t)$ reflects the fact that the effect of inelastic collisions is introduced by allowing the particle charge to change. The probability of a charge changing event is introduced via a Monte Carlo type method, where the probability of each process is taken proportional to the corresponding collision frequency. The electric field is assumed to be zero and the orbit integrator is the well-known Boris' algorithm [5, 6]. The code runs on a GPU, thus allowing calculations with a large number of particles in a short time using modest computational resources.

3. 1D case

Here we consider a 1D case and present some results that illustrate the basic features of the physical processes involved in the inelastic interaction of alpha particles with the plasma and neutral species. In what follows the 'neutral' density includes the contribution of all the species that can transfer electrons to the alpha particles, thus reducing their charge. These species appear in the LHS of equations (12.a) and (12.b) of [2] and also include He^+, which is not neutral. All these species are considered 'cold' in the sense that their average energy is much less than the alpha's and hence, their distribution function is assumed to be a delta function. There is very little information about the relative fractions of each of these species. We assumed a 30% fraction of D_0, D_2^0 and He^+ and a 10% fraction of He^0 but changing these fractions will not produce significant changes in the results because the reaction rates are similar (except perhaps for He^+) in the energy range where inelastic collisions can be important.

Figure 1(*a*) shows the evolution of a Gaussian alpha particle density profile in a plasma with uniform density ($n_e = 10^{20}\,\mathrm{m}^{-3}$), temperature ($T_e = 4$ keV) and magnetic field ($B = 5.3$ T) and a uniform neutral density equal to 0.35% of the electron density ($0.35\times10^{18}\,\mathrm{m}^{-3}$). All the alpha particles have an energy of 300 keV and Coulomb collisions are not included.

It is clear that charge changing processes produce the rapid diffusion of the alpha particles. Assuming that a standard diffusion process occurs, where the variance increases linearly in time, the diffusion coefficient is calculated as:

$$D = \frac{\langle\Delta r^2(t)\rangle - \langle\Delta r^2(0)\rangle}{2t}$$

where,

$$\langle\Delta r^2(t)\rangle = \frac{1}{N}\sum_{i=1}^{N}[r_i(t) - \bar{r}(t)]^2\,,$$

N is the total number of particles, $r_i(t)$ is the position of particle 'i' and $\bar{r}$ is the position of the center of mass. The result obtained from the simulation ($D = 20.0\ \mathrm{m^2 s^{-1}}$) agrees very well with the result obtained applying equation (11) of [2] ($D = 20.6\ \mathrm{m^2 s^{-1}}$).

Figure 1(*b*) was obtained using the same plasma and magnetic field parameters as in figure 1(*a*), and a non uniform neutral density profile which is the 1D equivalent to the one described in the next section ($n_{n0} = 10^{18}\,\mathrm{m}^{-3}$). We note that in this case the alpha particle distribution moves in the opposite direction to the neutral density gradient. For the parameters employed in this case the average velocity of the displacement, calculated from the position of the maximum at $t = 0$ and at $t = 1$ ms, is 50 m s^{-1}. This velocity is very sensitive to the neutral density gradient and decreases rapidly with it. The underlying microscopic mechanism responsible for this displacement was qualitatively explained in [2]. Since the distribution moves towards a region with lower neutral density the

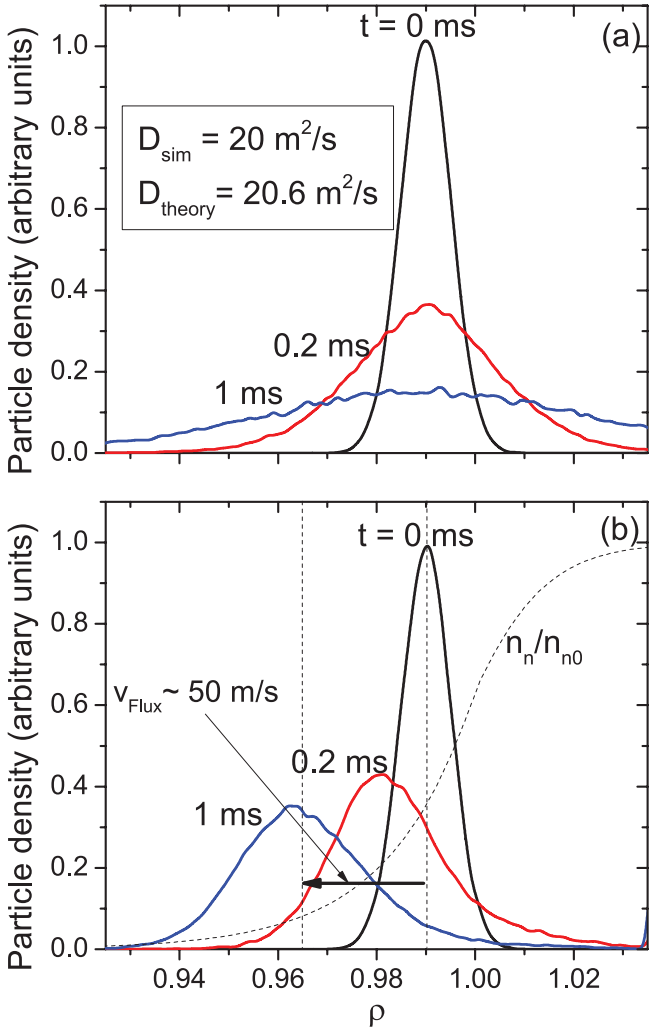

Figure 1. Evolution of an alpha particle Gaussian profile in a uniform plasma. The plasma conditions are $B = 5.3$ T, $T_e = 4$ keV and $n_e = 10^{20}$ m^{-3}. In (*a*) a uniform neutral density was used ($n_n = 0.35 \times 10^{18}$ m^{-3}) while in (*b*) a non uniform neutral density, with $n_{n0} = 10^{18}$ m^{-3}, was employed (shown with a dashed line).

diffusion (spreading) is reduced, compared with the case with uniform neutral density. We will see below that the inward motion produced by the neutral density gradient has important consequences for the transport of alpha particles in realistic 2D equilibria.

4. 2D Equilibrium and initial conditions

The 2D equilibrium employed was obtained from a numerical solution of the Grad–Shafranov equation that includes the vacuum region and the contribution of the external coils. The magnetic field and the basic plasma parameters are similar to those expected for the standard ITER inductive scenario [7]. In particular, we assumed a peak electron temperature (T_{e0}) of 25 keV, a peak electron density (n_{e0}) of 10^{20}m^{-3} and a vacuum toroidal magnetic field on axis of 5.3 T.

Figures 2–4, show, respectively, the cross section, with the flux surfaces and the chamber wall, the safety factor profile and the density and temperature profiles. In these figures the

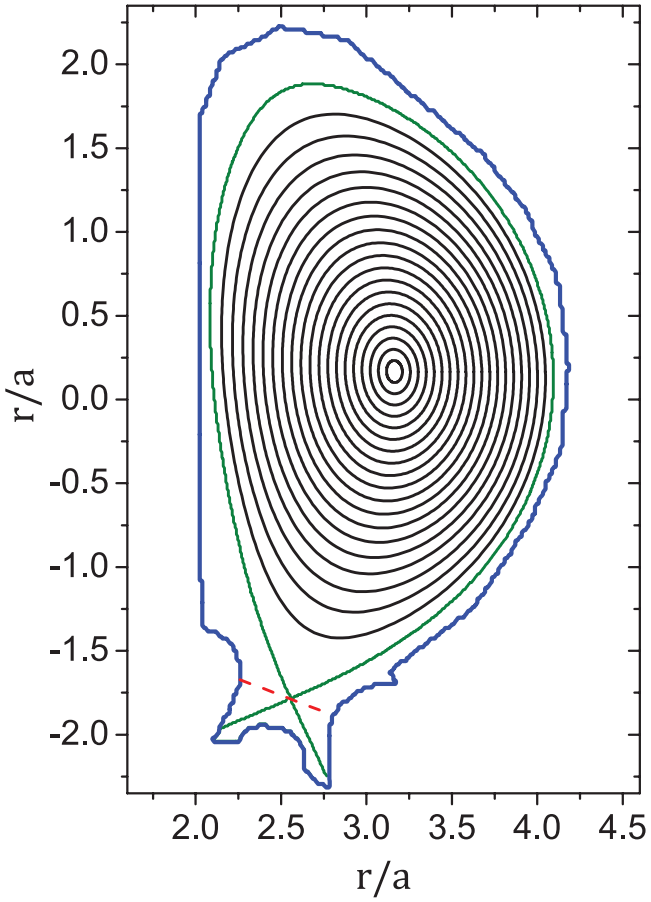

Figure 2. ITER vacuum vessel, separatrix and flux contours. Here, $a = 2$ m is the usual minor radius.

'radial' coordinate (ρ) is the square root of the toroidal flux. The details of the profiles in the outer plasma region are important for our calculation. Thus, we carefully matched different spatial dependencies to construct the plasma and neutral density profiles. For the electron density we assumed a uniform profile from the core to the pedestal (located at $\rho = 0.95$), a hyperbolic tangent from the pedestal to the separatrix and an exponential decay from the separatrix to the wall. In the region between the core and the pedestal the electron temperature was obtained by assuming an ideal gas law ($T_e = p/n_e$), where the pressure was obtained from the Grad-Shafranov equation. From the pedestal to the wall the assumptions used for the temperature are the same as those employed for the electron density.

Table 1 indicates the values of the electron density and temperature at specific points, where different functional dependencies are matched. The values at the separatrix and wall are similar to those proposed by Kukushkin *et al* [8, 9]. Finally for the neutral density we employed an exponential decay from the separatrix to the plasma core and a hyperbolic tangent from the separatrix to the wall. The values employed for the neutral density are similar to those obtained by Afanasyev *et al* [10] at the plasma core and by [11, 12] at the wall. Most of these functional assumptions are very similar to those employed in [13]. In what follows the quantity n_{n0} indicates the neutral density at the wall. We normally used $n_{n0} = 10^{18}$ m^{-3} (1% of the peak electron density) but

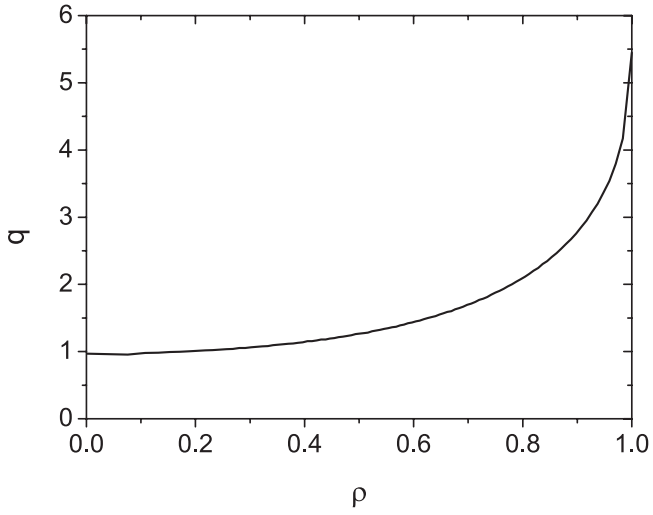

Figure 3. q profile of the equilibrium employed in the simulations.

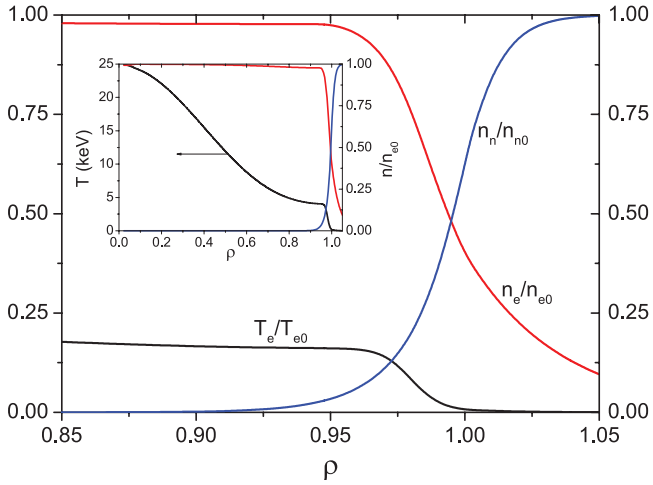

Figure 4. Plasma temperature and density profiles and neutral density profile normalized with T_{e0} (25 keV), n_{e0} (10^{20}m^{-3}) and n_{n0} (0.1%, 1% or 5% of n_{e0}), respectively.

Table 1. Values of the plasma density and temperature at selected points, where different functional dependencies are matched.

	Pedestal	Separatrix	Wall
T_e (keV)	4.0	0.17	0.01
$n_e(\times 10^{20})$ m^{-3}	1.0	0.40	0.1

$n_{n0} = 10^{17}$ m^{-3} and 5×10^{18} m^{-3} were also employed. These last values are unrealistic and were used to illustrate the effect of atomic processes in extreme cases.

Our simulations cover the region above the oblique dashed red line (see figure 2) that touches the lower tip of the separatrix (green), including the area between the separatrix and the wall. Particles that cross the dashed line are assumed to be lost to the divertor. The inner plasma region, with $\rho < 0.6$, is not included because the effect of inelastic collisions is negligible in this zone.

The alpha particles are loaded with a spatial distribution that has a Gaussian shape, with a its maximum at $\rho = 0$

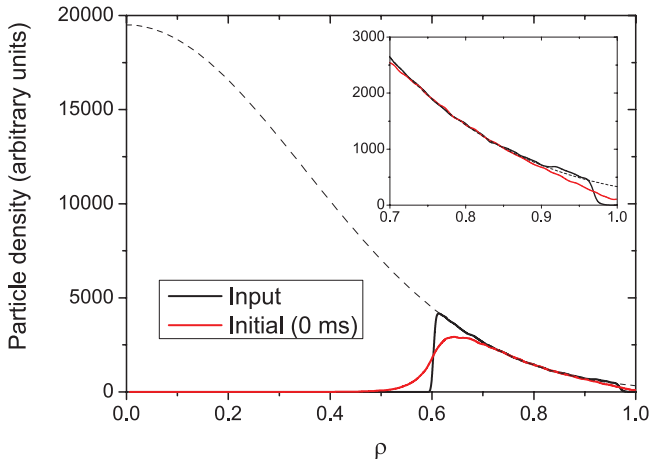

Figure 5. Input and initial conditions for the spatial alpha particle distribution. Initial conditions were obtained from the imput running the code for 1 ms without any collisions.

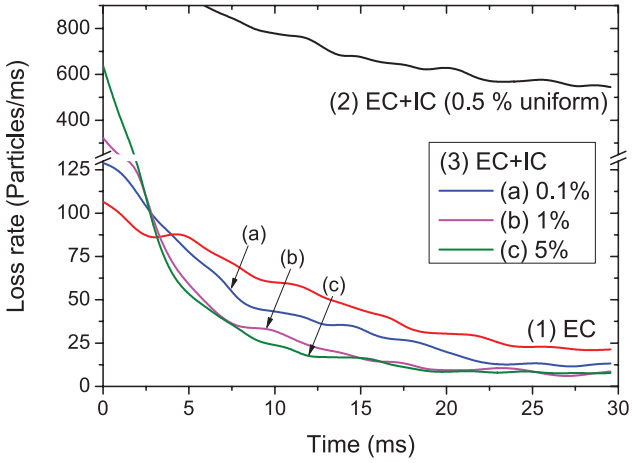

Figure 6. Loss rate of alpha particles as a function of time for different conditions. The simulations were performed with only elastic collisions (EC) and with both elastic and inelastic collisions (EC+IC).

and a normalized width of approximately 0.33 (black line in figure 5). Their initial velocity distribution is an isotropic slowing down distribution function. Starting with this initial condition, the code is run for 1 ms without collisions to eliminate poorly confined particles (first orbit losses). This results in a particle redistribution due to the curvature and ∇B drifts that produces the profile shown with a red line in figure 5.

The results presented below were obtained from simulations with 2–4 $\times 10^5$ particles that were followed for approximately 30 ms, or until they hit the wall or cross the dashed red line at the bottom of figure 2. Knowing the individual particle trajectories it is very simple to calculate all the quantities presented below. The particle loss rate is calculated by counting how many particles reach the wall or divertor in a given time interval and dividing by the time interval. A similar procedure is employed to calculate the energy loss rate (power), except that in this case we add the energies of all the lost particles. The density of alpha particles inside the separatrix is also calculated using the information about the individual particle positions. The curves shown in figure 8 represent flux

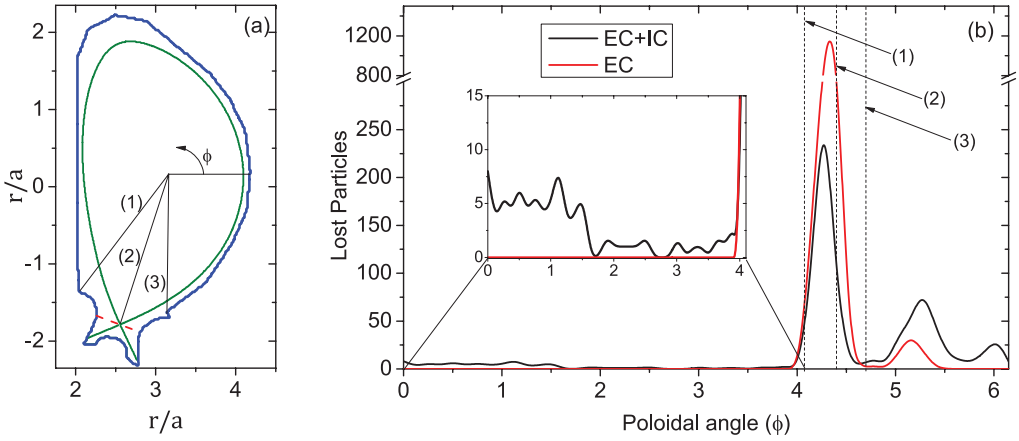

Figure 7. Poloidal distribution of lost particles with only elastic collisions (EC) and with both elastic and inelastic collisions (EC+IC) with $n_{n0}/n_{e0} = 1\%$.

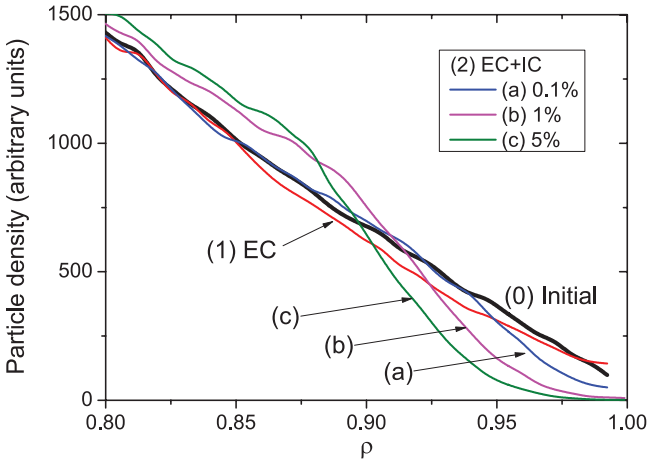

Figure 8. Initial (curve (0)) and final (curves (1) and (2) (a)–(c)) alpha particle density profiles.

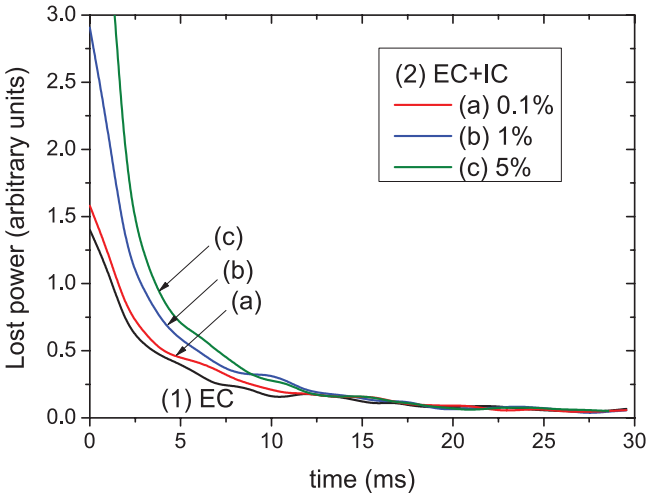

Figure 9. Total lost power as a function of time for different conditions. The simulations were performed with only elastic collisions (EC) and with both elastic and inelastic collisions (EC+IC).

surface averages because they were obtained by adding all the particles contained between two adjacent flux surfaces and dividing by the volume of this region. Finally, the poloidal distribution of lost particles (see figure 7) is easily reconstructed because we know the exact position where each particle hit the wall or divertor. Due to the short time of the simulations, which is nevertheless enough to reach a quasi stationary state, we do not introduce particle sources.

5. Results

Figure 6 shows the loss rate of alpha particles as a function of time for different conditions. The curve labelled (1) (EC, red) was obtained including only elastic (Coulomb) collisions, while all the others include both elastic and inelastic collisions (EC+IC). Curve (2) (EC+IC (0.5% uniform), black) was obtained with a uniform neutral density of 0.5×10^{18} m^{-3} (0.5% of the maximum electron density) while all the others, ((3), (a)–(c)) have the same type of profile as in figure 4, with $n_{n0}/n_{e0} = 0.1\%$ ((a), blue), 1% ((b), magenta) and 5% ((c), green).

Comparing curves (1) and (2), we note that including inelastic collisions with a uniform neutral density profile produces a very large increase in the loss rate. This is consistent with the large diffusion coefficient obtained for the 1D case (see section 3 above) and the results presented in [2] for parameters typical of the pedestal-edge-SOL regions.

When curve (1) is compared with the curves obtained with a non uniform neutral density profile ((3), (a)–(c)) two interesting features appear. The first one is that although the initial loss rate is higher when inelastic collisions are included, the stationary value is higher for the case which only has elastic collisions. The second one is that although the initial loss rate increases with the neutral density the stationary loss rate is approximately the same for the cases with $n_{n0} = 1$ and 5%. Finally, we note that the case with $n_{n0} = 0.1\%$ already shows a significant reduction of the loss rate. The lower loss rate obtained when inelastic collisions are included can be explained using the results presented in the previous section and in [2]. The inward particle flux produced by the neutral density gradient reduces the outward fluxes produced by elastic and inelastic collisions.

When there are only elastic collisions almost all the lost particles reach the divertor and there is a negligible flux to the wall. When inelastic collisions are added, the fraction of

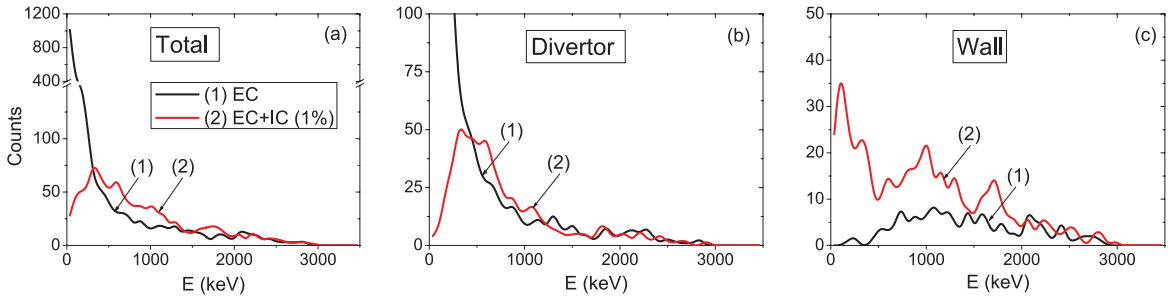

Figure 10. Energy distribution of lost particles with (EC+IC) and without (EC) inelastic collisions.

particles reaching the wall increases significantly. Considering the situation at the end of the simulations, when the initial transient has disappeared the fraction of lost particles reaching the wall is 5.6% when there are only elastic collisions and 32.1% when inelastic collisions, with $n_{n0}/n_{e0} = 1\%$, are added. The remaining particles cross the red dashed line of figure 2 and are assumed to be lost to the divertor. Figure 7 shows the poloidal distribution of the particles lost in the time interval $10\,\text{ms} < t < 30\,\text{ms}$ for two cases. The curve labelled EC (red) was obtained including only elastic collisions while the curve labelled EC+IC (black) includes both inelastic and elastic collisions, with $n_{n0}/n_{e0} = 1\%$. It is clear that the addition of inelastic collisions produces a significant increase in the number of lost particles that reach the lower half of the outer wall ($3\pi/2 < \phi < 2\pi$). This is very important because the additional particle (and energy, see below) flux could result in a larger than expected wall damage and particle recycling.

Figure 8 shows the initial alpha particle density profile ((0), black) and the final profiles obtained with elastic collisions alone ((1), red) and elastic plus inelastic collisions with different neutral densities ((2), (a)–(c)). We can see that elastic collisions produce a small reduction of the density near the edge but no significant changes in the shape of the profile. When inelastic collisions are added the shape of the density profile changes significantly. The region near the separatrix is depleted of alpha particles and a gentle maximum appears between $\rho = 0.8$ and $\rho = 0.9$. This maximum is produced by the inward flux described above and in [2] (see figure 7 of this reference). The maxima observed in [2] were sharper for three reasons: first, all the particles had the same energy; second, there were no elastic collisions; third, the particle profile was flatter than the one used here.

The particle loss rate is important but the energy loss rate, which is obtained by adding the energies of the lost particles, is also very important. Figure 9 shows the energy loss rate (power) for the same conditions as in figure 6. We note that although more particles are lost when there are only elastic collisions, the power loss rate at the end of the simulations, when the initial transients have disappeared, is approximately the same in all cases. This means that the average energy of the lost particles is larger when inelastic collisions are included. This behaviour can be explained by noting that the classical collision frequency increases as the energy of the alpha particle decreases while the inelastic collisions frequencies of the processes considered have maxima at energies between 100 and 1000 keV. Figure 10 shows the energy distribution of lost particles with, and without, inelastic collisions. When there are only elastic collisions the energy distribution of particles lost to the divertor (figure 10(*b*)) peaks at a very low energy while the distribution of those reaching the wall is very broad and has its maximum value above 1000 keV (figure 10(*c*)). Since the fraction of particles lost to the divertor is much larger than the fraction lost to the wall, the energy distribution of all the lost particles is very similar to the distribution of those reaching the divertor (figure 10(*a*)). When there are elastic and inelastic collisions the total (figure 10(*a*)) and divertor (figure 10(*b*)) distributions have maxima at around 400 keV while the distribution of those reaching the wall (figure 10(*c*)) has an absolute maximum at a very low energy and relative maxima at $E \simeq 1000$ keV and $E \simeq 1700$ keV.

6. Summary and conclusions

We presented the results of extensive numerical simulations of the effect of inelastic collisions on the transport of alpha particles. The equilibrium and plasma parameters employed correspond to the standard inductive scenario predicted for ITER. Our most important findings can be summarized as follows:

(i) The addition of inelastic collisions reduces the loss rate of alpha particles in the stationary regime. This is due to the existence of an inward flux produced by the gradient in the neutral density.
(ii) Including inelastic collisions changes significantly the spatial distribution of lost particles. In particular, the fraction of lost particles reaching the wall is much larger with inelastic collisions.
(iii) Although the particle lost rate is reduced when inelastic collisions are included, the energy loss rate (power) is approximately the same in all cases. This is due to a change in the energy distribution of the lost particles that results in a higher average energy of the lost particles in the case with inelastic collisions.

Since atomic processes change the spatial and energy distribution of the lost alpha particles it is clear that they should be included in the calculation of the energy and particle fluxes reaching the wall and the divertor. It is also clear that other atomic processes, for example the interaction of the alpha particles with high Z impurities (i.e. Tungsten), should be probably included and that more, and better data on the cross sections is needed. Our calculations did not include other

processes that will increase the flux of alpha particles from the core to the outer region, such as Alfvèn eigenmodes, sawteeth and microturbulence, and processes that specifically affect the plasma edge, such as toroidal field ripple and ELM control coils. These should be included in future studies but it is clear that if atomic processes produce very large changes when only classical collisions are included they will continue to do so if other loss mechanisms are added.

Finally, it would be very useful if our findings could be checked by performing dedicated experiments in present devices. One possibility would be to inject a He neutral beam with an energy of around 100 keV in the outer plasma region to try to establish a high enough alpha particle density in this region and measure the resulting losses and profiles. These experimental results could be then compared with the results obtained with our code for the same conditions.

Acknowledgments

This work was supported by the Comisión Nacional de Energía Atómica, CNEA (Controlled Nuclear Fusion Program) and Universidad Nacional de Cuyo (Grant 06/C416). The authors acknowledge the assistance of P.L. García-Martínez, who provided the 2D equilibrium employed. C.F.C. also acknowledges the support of the Consejo Nacional de Investigaciones Científicas y Técnicas (CONICET), Argentina.

References

[1] Fussmann G. 1997 Cross-field diffusion by charge changing process *Contrib. Plasma Phys.* **37** 363–75

[2] Clauser C.F. and Farengo R. 2015 Alpha particles diffusion due to charge changes *Phys. Plasmas* **22** 122502

[3] IAEA AMDIS ALADDIN Database (www-amdis.iaea.org/ALADDIN/)

[4] Ichimaru S. 1973 *Basic Principles of Plasma Physics: a Statistical Approach* (London: Benjamin)

[5] Boris J.P. and Shanny R. 1970 *4th Proc. of the Conf. on the Numerical Simulation of Plasmas (Naval Research Laboratory, Washington, DC)* (http://oai.dtic.mil/oai/oai?verb=getRecord&metadataPrefix=html&identifier=ADA023511)

[6] Qin H., Zhang S., Xiao J., Liu J., Sun Y. and Tang W.M. 2013 Why is Boris algorithm so good? *Phys. Plasmas* **20** 084503

[7] Shimada M. *et al* 2007 Chapter 1: overview and summary *Nucl. Fusion* **47** S1–7

[8] Kukushkin A.S., Pacher H.D., Pacher G.W., Janeschitz G., Coster D., Loarte A. and Reiter D. 2003 Scaling laws for edge plasma parameters in ITER from two-dimensional edge modelling *Nucl. Fusion* **43** 716–23

[9] Kukushkin A.S., Pacher H.D., Kotov V., Pacher G.W. and Reiter D. 2011 Finalizing the ITER divertor design: the key role of SOLPS modeling *Fusion Eng. Des.* **86** 2865–73

[10] Afanasyev V.I., Chernyshev F.V., Kislyakov A.I., Kozlovski S.S., Lyublin B.V., Mironov M.I., Melnik A.D., Nesenevich V.G., Petrov M.P. and Petrov S.Ya. 2010 Neutral particle analysis on ITER: present status and prospects *Nucl. Instruments Methods Phys.* A **621** 456–67

[11] Kukushkin A.S., Pacher H.D., Kotov V., Reiter D., Coster D. and Pacher G.W. 2005 Effect of neutral transport on ITER divertor performance *Nucl. Fusion* **45** 608–16

[12] Kotov V., Reiter D. and Kukushkin A.S. 2007 Numerical study of the ITER divertor plasma with the B2-EIRENE code package *Technical Report* (www.eirene.de/kotov_solps42_report.pdf)

[13] Mahdavi M.A., Maingi R., Groebner R.J., Leonard A.W., Osborne T.H. and Porter G. 2003 Physics of pedestal density profile formation and its impact on H-mode density limit in burning plasmas *Phys. Plasmas* **10** 3984